Journal of Non-Crystalline Solids 476 (2017) 75–80

Contents lists available at ScienceDirect

Journal of Non-Crystalline Solids

journal homepage: www.elsevier.com/locate/jnoncrysol

Glass-forming ability, thermal properties, and corrosion resistance of Fe-based (Fe, Ni, Mo, Cr)-P-C-B metallic glasses

Siwen Wang[a], Yanhui Li[a], Xuewei Wang[a], Shinichi Yamaura[a,b,c], Wei Zhang[a,b,*]

[a] Key Laboratory of Solidification Control and Digital Preparation Technology (Liaoning Province), School of Materials Science and Engineering, Dalian University of Technology, Dalian 116024, China
[b] Institute for Materials Research, Tohoku University, Sendai 980-8577, Japan
[c] Polytechnic University, Kodaira, Tokyo 187-0035, Japan

ARTICLE INFO

Keywords:
Fe-based bulk metallic glasses
Glass-forming ability
Supercooled liquid region
Corrosion resistance
Mechanical properties

ABSTRACT

Co-addition of appropriate Mo, Cr and Ni in the $Fe_{80}P_{12}C_4B_4$ alloy not only enhances the thermal stability of the supercooled liquid and glass-forming ability (GFA) but also reduces the glass transition temperature (T_g) of the Fe-based metallic glass. The $Fe_{55}Ni_{15}Cr_7Mo_3P_{12}C_4B_4$ bulk metallic glass (BMG) exhibits a low T_g of 690 K, large supercooled liquid region (ΔT_x) of 60 K, and high GFA with a critical diameter of 2.5 mm. The co-addition of Mo, Cr and Ni remarkably improves the corrosion resistance of the BMGs in 1 M HCl and 0.5 M H_2SO_4 solutions, which is superior compared to the SUS316L stainless steel. The alloys also possess high compressive yield strength of ~3.01 GPa with distinct plastic strain of ~1.2%. The good combination of low T_g, large ΔT_x, high GFA, excellent corrosion resistance and mechanical properties makes the developed $(Fe, Ni, Cr, Mo)_{80}P_{12}C_4B_4$ BMGs show great promise as anti-corrosion materials suitable for thermoplastic processing.

1. Introduction

Fe-based bulk metallic glasses (BMGs) are attractive in the BMG families from the standpoint of engineering applications owing to their high strength and hardness, good wear resistance, excellent soft magnetic properties, and relatively low material cost [1,2]. Over the last two decades, series of Fe-based BMGs have been developed, for instance, in Fe-(Al, Ga)-(P, C, B) [3], Fe-(Zr, Nb, Hf)-B [4], Fe-(Cr, Mo)-(P, C, B) [5], Fe-(Cr, Mo)-(Y, Ln)-(C, B) (Ln: lanthanides) [6], and Fe-P-C systems [7]. While most of them, especially for the Y- and Ln-free alloys, exhibit relatively low glass-forming ability (GFA) with a critical diameter for glass-formation (d_c) ≤ 3 mm. In addition, the Fe-based BMGs have a very limited plasticity at room temperature, which hinders their practical use as structural materials [8]. By taking the advantage of the viscous flow workability in the supercooled liquid region, the Fe-based BMGs can be made into functional devices with complex shapes by thermoplastic processing, and the metallic glass powders can be fabricated as protective coatings by thermal spraying, which extends the application areas of the Fe-based alloys [9,10]. In addition to the good GFA, the metallic glasses suitable for the thermoplastic processing should possess a low glass transition temperature (T_g) and a large supercooled liquid region (ΔT_x, the interval between the T_g and onset temperature of crystallization (T_x)) [10–12]. The alloy with a large ΔT_x usually possesses a low processing viscosity in the supercooled liquid state, which makes it easy for superplastic deformation or forming uniform and compact coatings [10,13,14]. A low T_g implies that the processing can be carried out at a low temperature, leading to the reductions of both equipment requirement and energy consume [10].

One of the typical applications for the thermoplastic processing of the metallic glasses is producing anti-corrosion bipolar plate for proton exchange membrane fuel cells by hot-pressing the Ni-based metallic glass sheet in the supercooled liquid state [13], or by thermal spray-coating the powders on Al-plate [14]. Although the excellent corrosion resistance of the Ni-based metallic glasses is beneficial to the service life of the bipolar plate in the acidic conditions, the low GFA, high T_g (~828 K), and high materials cost bring challenges to the industrialization. Fe-based metallic glasses with good corrosion resistance and proper properties for thermoplastic processing, i.e., low T_g and large ΔT_x, are hence expected to replace the Ni-based alloys in term of the low cost. While the previously developed Fe-based Fe-Cr-Mo-P-C-B [5], Fe-Cr-Mo-C-B-Y [15] and Fe-Co-B-Si-Nb-Cr [16] BMGs with high GFA, large ΔT_x and good corrosion resistance possess very high T_g (~936 K). The Fe-P-C [7] and Fe-P-C-B [17] BMGs show low T_g of ~690 K, whereas their ΔT_x are small (< 35 K), and the GFA and corrosion resistance are relatively poor. The Cr and Mo elements are

* Corresponding author.
E-mail address: wzhang@dlut.edu.cn (W. Zhang).

http://dx.doi.org/10.1016/j.jnoncrysol.2017.09.028
Received 8 June 2017; Received in revised form 7 September 2017; Accepted 11 September 2017
Available online 19 September 2017
0022-3093/

favorable to the improvement of corrosion resistance, but the excessive Cr/Mo leads to the increase of T_g and even deterioration of GFA [15,18]. It will be of significance to achieve the best combination of low T_g, high GFA, and excellent corrosion resistance by optimizing the Cr and Mo contents. In addition, substitution of Fe with proper Ni in the Fe-based BMGs is useful to reduce the T_g and increase the ΔT_x and GFA [12,19]. It is then predicted that combined addition of appropriate Mo, Cr and Ni is an effective way to obtain the Fe-based BMGs with high GFA, large ΔT_x, good corrosion and low T_g. In this work, an $Fe_{80}P_{12}C_4B_4$ metallic glass possessing a low T_g of 694 K were selected as the base alloy, and the effects of Mo, Cr and Ni additions on the thermal stability, GFA, corrosion resistance and mechanical properties were investigated.

2. Experimental procedure

Alloy ingots of (Fe, Ni, Cr, Mo)$_{80}P_{12}C_4B_4$ in at.% were prepared by induction melting the mixture of Fe (99.9 mass%), Mo (99.9 mass%), Cr (99.9 mass%), Ni (99.99 mass%), C (99.999 mass%), B (99.5 mass%) and Fe_3P precursor (99.9 mass%) under a high-purified argon atmosphere. The mass losses were < 0.2 mass%. Ribbons with a width of 2 mm and thicknesses of 20 μm were prepared by single-roller melt spinning with a linear velocity for copper wheel of 40 m/s. Cylindrical rods with diameters of 1–3 mm were fabricated by copper mold casting. The structure of the samples was examined by X-ray diffraction (XRD) with Cu-K_α radiation using a D8 Focus (Bruker). The thermal properties associated with the glass transition, supercooled liquid region and crystallization of the samples were measured by differential scanning calorimetry (DSC, Q100, TA Ins.) from 373 to 873 K at a heating rate of 0.67 K/s. The ribbons were heated to the respective onset temperature of each crystallization peak under the same heating rate as the DSC test, held isothermally for 60 s, and subsequently quenched into water to study the crystallization products corresponding to each crystallization peak. A series of isothermal DSC measurements were carried out at temperatures between 688 and 743 K to investigate the crystallization behavior. The ribbons were first heated to the desired annealing temperature at a heating rate of 0.67 K/s and then held isothermally for a certain period of time until the completion of crystallization. The liquidus temperature (T_l) was measured with a differential thermal analyzer (DTA, Q600, TA Ins.) at a heating rate of 0.33 K/s. At least three tests were repeated for each determination of the thermal parameters. The maximum variation in the temperature measurements is less than ± 1 K. The corrosion behaviors of the alloys were evaluated by electrochemical measurements and immersion tests in 1 M HCl and 0.5 M H_2SO_4 solutions open to air, respectively. The samples (ribbons for electrochemical tests and φ1.5 mm rods for immersion) were firstly mechanically polished and subsequently exposed to air for 24 h for a consistent surface condition. The electrochemical measurements were conducted in a three-electrode cell with a platinum counter electrode and an Ag/AgCl reference electrode at 298 K. Potentiodynamic polarization curves were measured using electrochemical workstation (Interface1000, Gamry) at a potential sweep rate of 50 mV/min after open-circuit immersion of samples for about 20 min when the open-circuit potentials became almost steady. The corrosion rates were estimated from the weight losses of the samples after immersion in the solutions at 298 K for 168 h. The mechanical properties of the alloys were measured using an Instron 5581 mechanical testing machine under the compressive load. The gauge dimension for the mechanical test specimen was 2 mm in diameter and 4 mm in height, and the strain rate was fixed as $5.0 \times 10^{-4}\ s^{-1}$. The fracture morphology of the specimen were observed by scanning electron microscope (SEM, JSM-5600LV, JEOL). At least three samples for each composition were repeated in the corrosion and mechanical measurements.

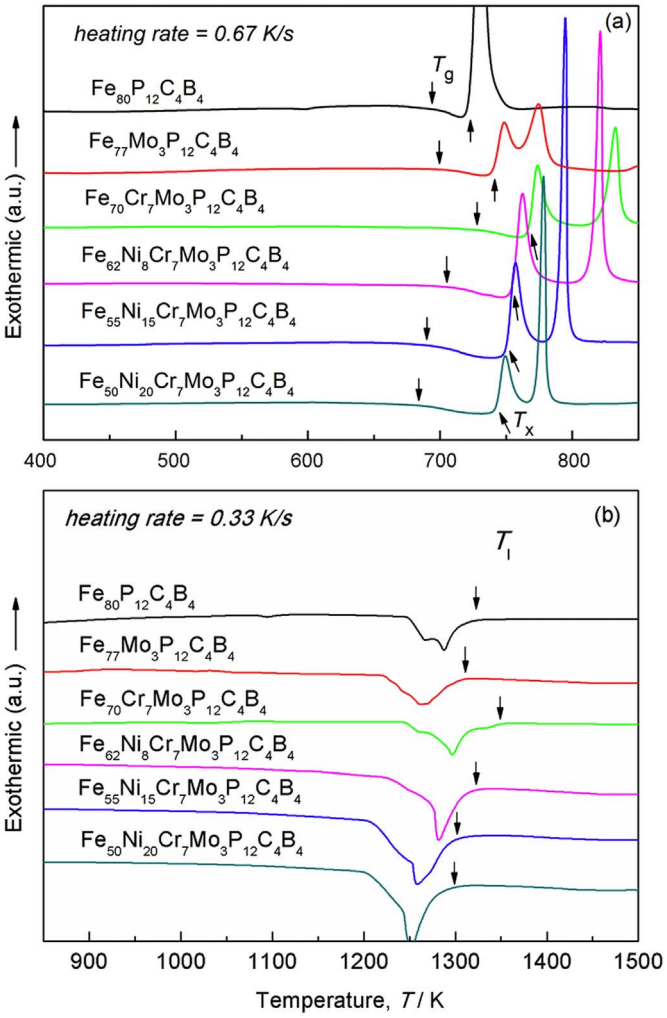

Fig. 1. DSC (a) and DTA (b) curves of (Fe, Ni, Mo, Cr)$_{80}P_{12}C_4B_4$ metallic glasses.

3. Results

A fully glassy structure was confirmed for the as-spun (Fe, Ni, Cr, Mo)$_{80}P_{12}C_4B_4$ ribbon samples according to the XRD results. Fig. 1 shows the DSC (a) and DTA (b) curves of the metallic glasses, and the T_g, T_x and T_l are marked in the figures by arrows. During the continuous heating, the alloys all exhibit a clear endothermic glass transition followed by a supercooled liquid region, and then exothermic peaks corresponding to crystallization (see Fig. 1(a)). The additions of 3 at.% Mo and 3 at.% Mo + 7 at.% Cr shift the T_g and T_x of the alloy towards higher temperatures, and extend the ΔT_x from 29 to 37 and 42 K, respectively. The further addition of 8–20 at.% Ni in the $Fe_{70}Cr_7Mo_3P_{12}C_4B_4$ alloy reduces the T_g to 684 K without greatly decreasing the T_x, and hence extends the ΔT_x up to 60 K. The extended ΔT_x suggests that the co-addition of Mo, Cr and Ni improves the thermal stability of the supercooled liquid of the alloy effectively. From the DTA curves, it is detected that the addition of Mo + Cr increases the T_l of the base alloy from 1323 to 1349 K, while co-addition of Mo, Cr and Ni decreases the T_l to 1299 K (see Fig. 1(b)). Table 1 lists the T_g, ΔT_x, T_l, and GFA indicators, i.e., T_{rg} ($= T_g / T_l$) [20], γ ($= T_x / (T_l + T_g)$) [21] and S ($= \Delta T_x / (T_l - T_g)$) [10] values of the present alloys. It is seen that the ΔT_x, γ, and S values rise simultaneously with the addition of Mo, Cr and Ni until the Ni content reaches 20 at.%, which indicates an increased GFA.

Cylindrical rods with different diameters were produced by copper mold casting to evaluate the GFA of the (Fe, Ni, Cr, Mo)$_{80}P_{12}C_4B_4$ alloys. Fig. 2 presents the XRD patterns of the as-cast rods with diameters

Table 1
Summary of thermal parameters and critical diameters (d_c) of (Fe, Ni, Mo, Cr)$_{80}$P$_{12}$C$_4$B$_4$ metallic glasses. The T_g, ΔT_x, and T_l values were derived from the DSC traces under a heating rate of 0.67 K/s.

Alloys (at.%)	T_g (K)	ΔT_x (K)	T_l (K)	T_{rg}	γ	S	d_c (mm)
$Fe_{80}P_{12}C_4B_4$	694 ± 1	29 ± 2	1323 ± 1	0.525	0.359	0.046	< 1.0
$Fe_{77}Mo_3P_{12}C_4B_4$	702 ± 1	37 ± 2	1311 ± 1	0.535	0.367	0.061	< 1.0
$Fe_{70}Cr_7Mo_3P_{12}C_4B_4$	728 ± 1	42 ± 2	1349 ± 1	0.540	0.371	0.068	1.5
$Fe_{62}Ni_8Cr_7Mo_3P_{12}C_4B_4$	705 ± 1	51 ± 2	1323 ± 1	0.533	0.373	0.083	2.0
$Fe_{55}Ni_{15}Cr_7Mo_3P_{12}C_4B_4$	690 ± 1	60 ± 2	1302 ± 1	0.530	0.377	0.098	2.5
$Fe_{50}Ni_{20}Cr_7Mo_3P_{12}C_4B_4$	684 ± 1	58 ± 2	1299 ± 1	0.527	0.374	0.094	2.0

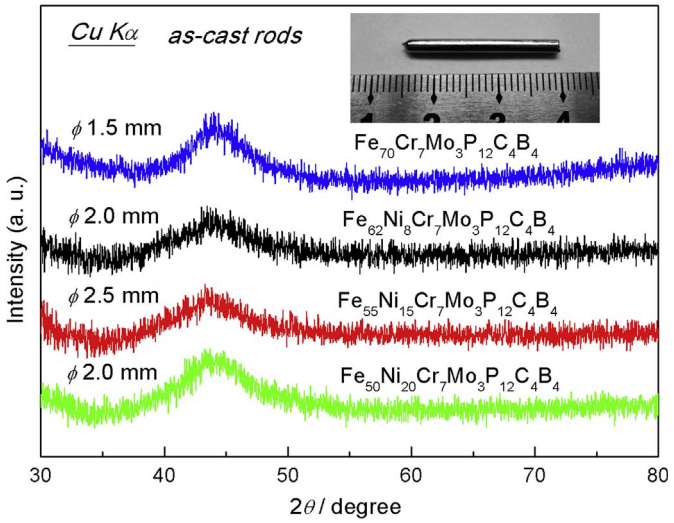

Fig. 2. X-ray diffraction patterns of as-cast (Fe, Ni, Mo, Cr)$_{80}$P$_{12}$C$_4$B$_4$ alloy rods with diameters of 1.5–2.5 mm. Inset is the outer appearance of as-cast $Fe_{55}Ni_{15}Cr_7Mo_3P_{12}C_4B_4$ alloy rod with a diameter of 2.5 mm.

of 1.5–2.5 mm. All patterns consist of only a series of broad diffraction maxima without any detectable sharp Bragg peak, indicating that the samples have a fully glassy structure. The inset in Fig. 2 shows the outer surface of the as-cast $Fe_{55}Ni_{15}Cr_7Mo_3P_{12}C_4B_4$ BMG rod with a diameter of 2.5 mm. The sample exhibits a very smooth surface with shiny luster. The d_c of the alloy series are listed in Table 1. It is seen that addition of 3 at.% Mo + 7 at.% Cr raises the d_c of the base alloy from < 1 to 1.5 mm. Subsequent addition of 8–20 at.% Ni further increases the d_c, and the $Fe_{55}Ni_{15}Cr_7Mo_3P_{12}C_4B_4$ BMG possesses the largest d_c of 2.5 mm. The results reveal that the co-addition of proper Mo, Cr and Ni enhances the GFA of the alloy greatly. As shown in Fig. 3, the d_c, ΔT_x, γ and s values of the $Fe_{70-x}Ni_xCr_7Mo_3P_{12}C_4B_4$ alloys go upward simultaneously with increasing x from 0 to 15 and then decline slightly with further increasing x to 20, while the T_{rg} decreases monotonously with increasing x from 0 to 20. The change of d_c with alloy composition shows better correlations with ΔT_x, γ, and S values than T_{rg}.

Fig. 4 displays the potentiodynamic polarization curves of the (Fe, Ni, Cr, Mo)$_{80}$P$_{12}$C$_4$B$_4$ metallic glasses in 1 M HCl (a) and 0.5 M H_2SO_4 (b) solutions open to air at 298 K. The curves of SUS316L stainless steel are also shown for comparison. The electrochemical parameters including the corrosion potential (E_{corr}) and corrosion current density (I_{corr}) derived from the polarization curves by Tafel law [22] are listed in Table 2. In 1 M HCl solution (see Fig. 4(a) and Table 2), the $Fe_{80}P_{12}C_4B_4$ alloy undergoes an active dissolution and no obvious passivation region can be seen. Single addition of 3 at.% Mo raises the E_{corr} of the base alloy from − 303 ± 8 to − 284 ± 13 mV, and lowers the I_{corr} from (1.51 ± 0.11) × 10^{-3} to (8.82 ± 0.23) × 10^{-5} A/cm^2. Co-addition of 3 at.% Mo + 7 at.% Cr further increases the E_{corr} to − 88 ± 11 mV and lowers the I_{corr} to (2.58 ± 0.26) × 10^{-6} A/cm^2. In addition, a pronounced spontaneous passivation and followed a large passive region with a passivation current density (I_{pass}) of ~10^{-5} A/cm^2 can be observed in the curve, revealing that the Cr addition improves the corrosion resistance significantly. Subsequent addition of 8–20 at.% Ni continuously shifts the E_{corr} towards nobler potential and decreases the I_{corr} greatly. The alloys containing 15 and 20 at.% Ni possesses high E_{corr} of 51 ± 8 and 66 ± 10 mV, and low I_{corr} of (4.10 ± 0.11) and (3.29 ± 0.21) × 10^{-7} A/cm^2, respectively. The I_{pass} of the alloy with 20 at.% Ni shows a distinct reduction as well. The results in H_2SO_4 solution are similar to those in HCl solution, i.e., the additions of Mo, Cr and Ni enhance the corrosion resistance of the alloy effectively by gradually increasing the E_{corr} and lowering the I_{corr} and I_{pass} (see Fig. 4(b) and Table 2). Although the (Cr, Mo)-added alloy shows an active/passive transition revealed by a current density peak before passivation, the alloys with Ni content ≥ 15 at.% exhibit typical self-passivation behavior. The nobler E_{corr} and lower I_{corr} and I_{pass} suggest that the present alloys with co-addition of Mo, Cr, and Ni possess superior corrosion resistance compared to that of the SUS316L

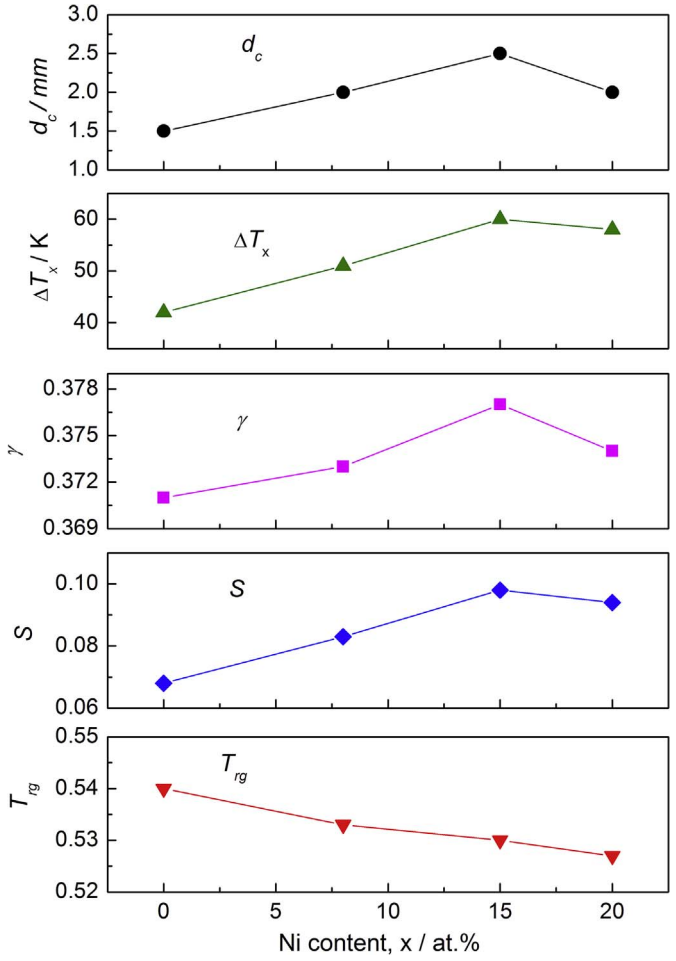

Fig. 3. Changes of d_c, ΔT_x, γ and s values of $Fe_{70-x}Ni_xCr_7Mo_3P_{12}C_4B_4$ (x = 0–20) metallic glasses as a function of Ni content.

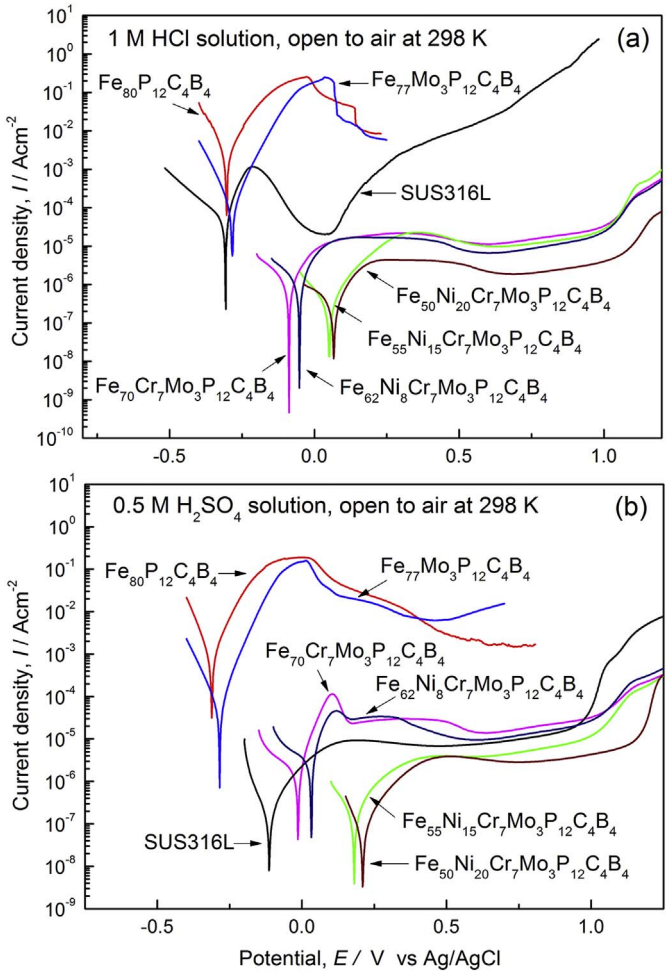

Fig. 4. Potentiodynamic polarization curves of (Fe, Ni, Mo, Cr)$_{80}P_{12}C_4B_4$ metallic glasses in 1 M HCl (a) and 0.5 M H_2SO_4 (b) solutions at 298 K open to air. The curves of SUS316L stainless steel are shown for comparison.

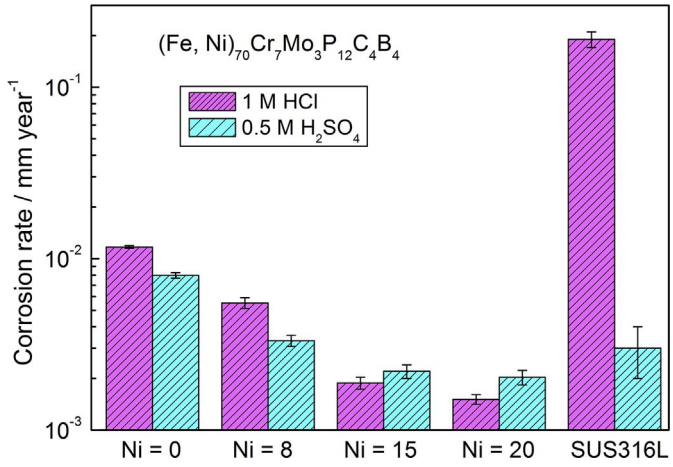

Fig. 5. Corrosion rates of (Fe, Ni)$_{70}Cr_7Mo_3P_{12}C_4B_4$ BMG rods and SUS316L stainless steel in 1 M HCl and 0.5 M H_2SO_4 solutions open to air for 168 h at 298 K, respectively.

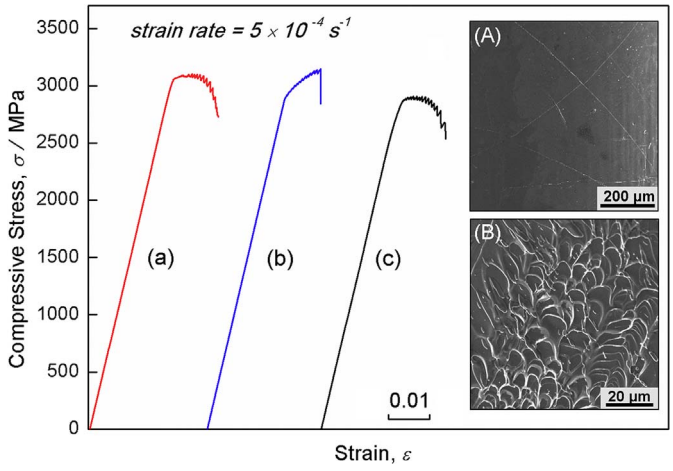

Fig. 6. Compressive stress-strain curves of as-cast $Fe_{62}Ni_8Cr_7Mo_3P_{12}C_4B_4$ (a), $Fe_{55}Ni_{15}Cr_7Mo_3P_{12}C_4B_4$ (b), and $Fe_{50}Ni_{20}Cr_7Mo_3P_{12}C_4B_4$ (c) glassy rods with a diameter of 2.0 mm. The insets are SEM micrographs of lateral (A) and fracture (B) surfaces morphology of the cracked $Fe_{50}Ni_{20}Cr_7Mo_3P_{12}C_4B_4$ sample.

stainless steel in both HCl and H_2SO_4 solutions. Fig. 5 presents the corrosion rates of the (Fe, Ni)$_{70}Cr_7Mo_3P_{12}C_4B_4$ BMGs and SUS316L stainless steel estimated form the weights losses after immersion in 1 M HCl and 0.5 M H_2SO_4 solutions, respectively. It is seen that the corrosion rates of the BMGs decrease significantly with Ni content increasing. The corrosion rates of the $Fe_{50}Ni_{20}Cr_7Mo_3P_{12}C_4B_4$ BMG in 1 M HCl and 0.5 M H_2SO_4 solutions lower to $(1.5 \pm 0.1) \times 10^{-3}$ and $(2.1 \pm 0.2) \times 10^{-3}$ mm/year, respectively. In consistent with the electrochemical results, the BMGs with the co-addition of Ni, Cr and Mo possess lower corrosion rates than those of the SUS316L stainless steel, revealing better corrosion resistance (see Figs. 4 and 5).

Fig. 6 shows the compressive stress-strain curves of the as-cast (Fe, Ni)$_{70}Cr_7Mo_3P_{12}C_4B_4$ BMG rods with a diameter of 2.0 mm. Under loading, the alloys all exhibit an initial elastic deformation with an elastic strain around 2%, and then begin to yield, followed by a distinct plastic deformation and final failure. The BMGs possess high compressive yield strength ($\sigma_{c,y}$) of (2.79 ± 0.10)–(3.01 ± 0.13) GPa, fracture strength ($\sigma_{c,f}$) of (2.92 ± 0.09)–(3.13 ± 0.11) GPa, and plastic strain ($\varepsilon_{c,p}$) of (0.8 ± 0.1)–(1.2 ± 0.2) %. As shown in the inset (A) of Fig. 6, some shear bands with inclination angle of about 45° to the direction of the applied compressive load can be observed on the lateral surface of the deformed $Fe_{55}Ni_{15}Cr_7Mo_3P_{12}C_4B_4$ specimen, which is suggested to contribute to the achievement of the plastic strain during compression. In addition, the fracture surface exhibits a well-

Table 2
Summary of electrochemical parameters of (Fe, Ni, Mo, Cr)$_{80}P_{12}C_4B_4$ metallic glasses. E_{corr} and I_{corr} represent the corrosion potential and corrosion current density, respectively.

Alloys (at.%)	1 M HCl		0.5 M H_2SO_4	
	E_{corr} (mV)	I_{corr} (A/cm^2)	E_{corr} (mV)	I_{corr} (A/cm^2)
$Fe_{80}P_{12}C_4B_4$	− 303 ± 8	$(1.51 \pm 0.11) \times 10^{-3}$	− 312 ± 7	$(7.79 \pm 0.15) \times 10^{-4}$
$Fe_{77}Mo_3P_{12}C_4B_4$	− 284 ± 13	$(8.82 \pm 0.23) \times 10^{-5}$	− 281 ± 10	$(2.47 \pm 0.21) \times 10^{-5}$
$Fe_{70}Cr_7Mo_3P_{12}C_4B_4$	− 88 ± 11	$(2.58 \pm 0.26) \times 10^{-6}$	− 13 ± 9	$(1.76 \pm 0.23) \times 10^{-6}$
$Fe_{62}Ni_8Cr_7Mo_3P_{12}C_4B_4$	− 52 ± 6	$(1.21 \pm 0.13) \times 10^{-6}$	37 ± 5	$(7.28 \pm 0.26) \times 10^{-7}$
$Fe_{55}Ni_{15}Cr_7Mo_3P_{12}C_4B_4$	51 ± 8	$(4.10 \pm 0.11) \times 10^{-7}$	183 ± 7	$(4.81 \pm 0.11) \times 10^{-7}$
$Fe_{50}Ni_{20}Cr_7Mo_3P_{12}C_4B_4$	66 ± 10	$(3.29 \pm 0.21) \times 10^{-7}$	209 ± 11	$(4.56 \pm 0.19) \times 10^{-7}$
SUS316L	− 308 ± 9	$(3.75 \pm 0.16) \times 10^{-5}$	− 114 ± 7	$(5.07 \pm 0.20) \times 10^{-7}$

Table 3
The thermal properties, critical diameters (d_c), compressive yield strength ($\sigma_{c,y}$), fracture strength ($\sigma_{c,f}$), and plastic strain ($\varepsilon_{c,p}$) of some typical Fe-based BMGs with high corrosion resistance.

Alloy (at.%)	T_g (K)	ΔT_x (K)	d_c (mm)	$\sigma_{c,y}$ (GPa)	$\sigma_{c,f}$ (GPa)	$\varepsilon_{c,p}$ (%)
$Fe_{75}Cr_5P_9C_7B_4$ [25]	733	33	2.0	–	3.19	0
$Fe_{43}Cr_{16}Mo_{16}C_{15}B_{10}$ [26]	870	66	1.5	2.4	–	1.7
$Fe_{43}Cr_{16}Mo_{16}P_{10}C_{10}B_5$ [5]	860	70	2.2	–	–	–
$Fe_{29.4}Cr_{29.4}Mo_{14.7}C_{14.7}B_{9.8}Y_2$ [15]	936	79	3.0	–	3.91	0
$Fe_{41}Co_{28}B_{18}Si_5Nb_4Cr_4$ [16]	833	41	3.0	–	–	–
$Fe_{41}Cr_{15}Mo_{14}Co_7C_{15}B_6Y_2$ [24]	853	53	14.0	–	3.55	0
$Fe_{62}Ni_8Cr_7Mo_3P_{12}C_4B_4$	705	51	2.0	3.01	3.10	1.1
$Fe_{55}Ni_{15}Cr_7Mo_3P_{12}C_4B_4$	690	60	2.5	2.80	3.13	0.8
$Fe_{50}Ni_{20}Cr_7Mo_3P_{12}C_4B_4$	684	58	2.0	2.79	2.92	1.2

developed vein pattern (see inset (B) of Fig. 6), which is typical of the tough BMGs.

Table 3 summaries the thermal properties, GFA, and mechanical properties of some typical Fe-based BMGs with high corrosion resistance [5,15,16,23–25]. The present $(Fe, Ni)_{70}Cr_7Mo_3P_{12}C_4B_4$ BMG possesses much lower T_g of 684–705 K compared to those of 733–936 K for the other listed alloys, while the strength is comparable. More importantly, the present BMGs simultaneously exhibit low T_g, large ΔT_x, high GFA and excellent corrosion resistance, which makes them potential candidates for anti-corrosion materials suitable for the thermoplastic processing.

4. Discussion

As described above, the additions of Mo, Cr and Ni in the $Fe_{80}P_{12}C_4B_4$ metallic glass make significant increases of the GFA and ΔT_x. It is well known that a certain mismatch of atomic sizes and large negative heat of mixing (ΔH^{mix}) among the constituent elements in a multi-component system are beneficial to the GFA [26]. In the present Fe-Ni-Cr-Mo-P-C-B alloy system, the atomic radii (r) changes in the order of r_{Mo} (0.136 nm) > r_{Ni} and r_{Cr} (0.125 nm) > r_{Fe} (0.124 nm) > r_P (0.109 nm) > r_B (0.090 nm) > r_C (0.077 nm) [27]. It is then anticipated that the suitable combination of atoms in different sizes produces an efficiently packed local structure, which is often associated with low energy and high viscosity of the liquids, leading to enhanced GFA. In addition, the ΔH^{mix} between the atomic pairs of Mo-P, Mo-C, Mo-B, Cr-P, Cr-C, Cr-B, Ni-P, Ni-C, and Ni-B are − 53.5, − 67, − 34, − 49.5, − 61, − 31, − 34.5, − 39, and − 24 kJ/mol, respectively [27]. Accordingly, the added Mo, Cr, and Ni elements bring new strong chemical affinities between the atomic pairs in the alloy system, which improve the local packing efficiency and restrain the long-range diffusion of atoms, resulting in the improvement of the GFA.

The $Fe_{80}P_{12}C_4B_4$ metallic glass exhibits only one exothermic peak in the DSC trace, and the alloys containing (Ni, Cr, Mo) show two peaks (see Fig.1(a)), which implies that the (Ni, Cr, Mo) addition may change the crystallization process of the alloys into multi stages. The crystallization products corresponding to the respective crystallization peak were investigated. As shown in Fig. 7(a), for the $Fe_{80}P_{12}C_4B_4$ alloy, the mixed phases of α-Fe + $Fe_3(B, P)$ are formed at 723 K (= T_x) and keep stable at 753 K (= T_x + 30 K). For the $Fe_{70}Cr_7Mo_3P_{12}C_4B_4$ alloy, the $(Fe, Cr, Mo)_4(P, C)$ phase is primarily precipitated in the amorphous matrix at 770 K (= T_x), and transforms to $Fe_3(B, C)$ + $Fe_3(B, P)$ phases at 826 K (corresponding to the onset temperature of the second crystallization peak). The changed crystallization products with temperature increase confirm that the alloy containing (Cr, Mo) possesses a multi-stage crystallization behavior. The crystallization activation energy is an important kinetic parameter reflecting the thermal stability of the supercooled liquid of metallic glasses. The Arrhenius equation $K_T = K_0 \exp(-E_c / RT)$ was taken to calculate the activation energy for crystallization, where K_T is the temperature-dependent kinetic constant which can be calculated by the Johnson-Mehl-Avrami

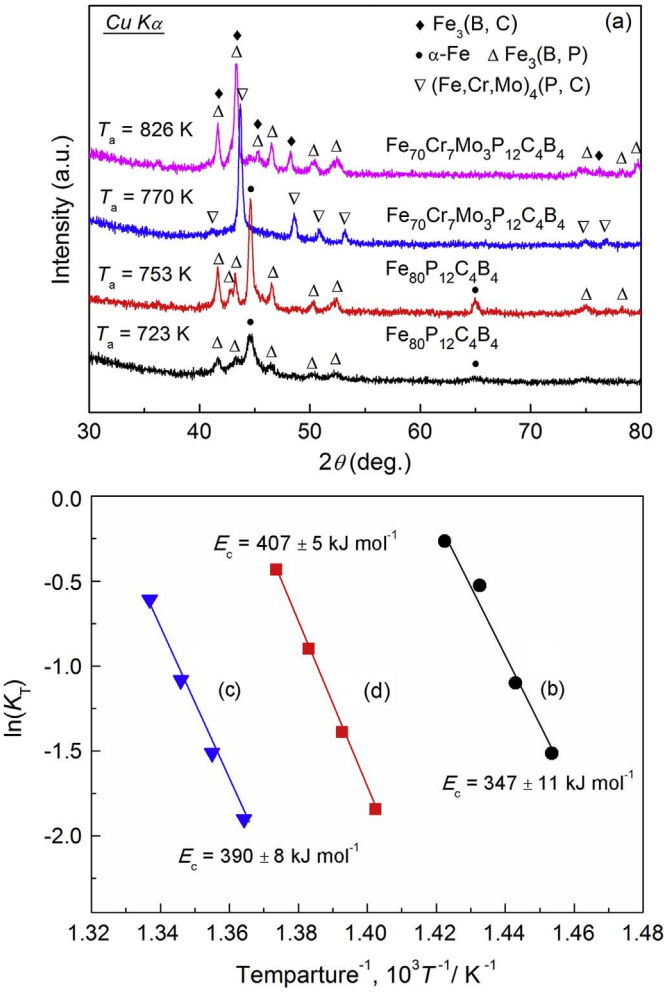

Fig. 7. X-ray diffraction patterns of $Fe_{80}P_{12}C_4B_4$ and $Fe_{70}Cr_7Mo_3P_{12}C_4B_4$ metallic glasses after annealing for 60 s at different temperatures (T_a) (a), and Arrhenius plots for the isothermal activation energy (E_c) of $Fe_{80}P_{12}C_4B_4$ (b) $Fe_{70}Cr_7Mo_3P_{12}C_4B_4$ (c), and $Fe_{55}Ni_{15}Cr_7Mo_3P_{12}C_4B_4$ (d) metallic glasses, respectively.

equation [28], K_0 is a constant, E_c is the apparent activation energy for crystallization, and T is the isothermal temperature. The Arrhenius plots for isothermal crystallization, i.e., ln (K_T) vs 1000 T^{-1} of the $(Fe, Ni, Cr, Mo)_{80}P_{12}C_4B_4$ metallic glasses are shown in Fig. 7. By linear fitting the data, the E_c corresponding to the first crystallization calculated from the slopes of the straight lines are 347 ± 11, 390 ± 8, and 407 ± 5 kJ/mol for $Fe_{80}P_{12}C_4B_4$, $Fe_{70}Cr_7Mo_3P_{12}C_4B_4$ and $Fe_{55}Ni_{15}Cr_7Mo_3P_{12}C_4B_4$ alloys, respectively. The E_c rises gradually with the additions of (Mo, Cr) and (Ni, Cr, Mo), which shows a good correlation with the ΔT_x. The increased E_c indicates that the nucleation and growth of the crystalline phases become more difficult during the

crystallization process, leading to the enhancement of the stability of the supercooled liquid.

It has been reported that Cr is one of the key passivating elements responsible for the high corrosion resistance of Fe-based metallic glasses [29]. Mo can prevent the dissolution of Cr during passivation and cause the enrichment of Cr in the passive film, hence stabilize the passive film [2]. It is reasonable that the alloy with co-addition of Mo + Cr shows much better corrosion resistance than those of the base and single Mo-added alloy (see Fig. 4). The Ni tends to form compact oxide layer when the alloy surface is passivated. The higher content of Ni results in a more compact oxide layer [30]. In addition, the standard equilibrium electrode potential of Fe/Fe^{2+} and Ni/Ni^{2+} are -0.440 V_{SHE} and -0.250 V_{SHE}, respectively [31]. A higher electrode potential means that the alloy is more difficult to dissolve. The alloys with higher Ni content exhibit enhanced corrosion resistance. Therefore, the co-addition of Mo + Cr + Ni facilitates the formation of a stable and protective passive film on the surface of the alloys, which effectively prevents the dissolution of the alloys in HCl and H_2SO_4 solutions, leading to the significant enhancement of the corrosion resistance.

The Fe-based BMGs usually failure immediately after reaching their elastic limit without yielding and plastic deformation [8]. The present $(Fe, Ni)_{70}Cr_7Mo_3P_{12}C_4B_4$ BMGs exhibit typical yielding and distinct plastic strain of ~1.2%. This is presumably attributable to their low T_g, which is closely related to the shear modulus [32,33]. The low T_g reflects the decrease in the shear modus, hence the shear deformation of the BMGs could easily occur, which results in an improved plasticity.

5. Conclusions

In this study, a series of $(Fe, Ni, Cr, Mo)_{80}P_{12}C_4B_4$ BMGs with low T_g, large ΔT_x, high GFA, good corrosion resistance, and high strength were developed. The results are summarized as follows:

(1) The addition of 3 at.% Mo and 7 at.% Cr improves the stabilization of supercooled liquid and GFA of the $Fe_{80}P_{12}C_4B_4$ alloy. The ΔT_x increases from 29 to 42 K, and the BMG rod with a diameter of 1.5 mm can be obtained.
(2) The addition of 8–20 at.% Ni in the $Fe_{70}Cr_7Mo_3P_{12}C_4B_4$ alloy not only raises the ΔT_x and d_c but also reduces the T_g. The $Fe_{55}Ni_{15}Cr_7Mo_3P_{12}C_4B_4$ BMG possesses the largest ΔT_x of 60 K and d_c of 2.5 mm as well as a low T_g of 690 K.
(3) The additions of Mo, Cr and Ni remarkably enhance the corrosion resistance of the base alloy in 1 M HCl and 0.5 M H_2SO_4 solutions. The alloys with co-addition of Mo, Cr, and Ni show superior corrosion resistance compared to that of the SUS316L stainless steel.
(4) The $(Fe, Ni)_{70}Cr_7Mo_3P_{12}C_4B_4$ BMGs exhibit good mechanical properties, i.e., high $\sigma_{c,y}$ of 2.79 to 3.01 GPa with $\varepsilon_{c,p}$ of 0.8 to 1.2%.

Acknowledgement

This work was supported by the National Natural Science Foundation of China [Grant Nos. 51571047, 51271043], the Natural Science Foundation of Liaoning Province [Grant No. 201602184], and the Advanced Materials Development and Integration of Novel Structured Metallic and Inorganic Materials from the Ministry of Education, Science, Sports, and Culture of Japan.

References

[1] A. Inoue, Stabilization of metallic supercooled liquid and bulk amorphous alloys, Acta Mater. 48 (2000) 276–306.
[2] C. Suryanarayana, A. Inoue, Bulk Metallic Glasses, CRC, Boca Raton, 2011.
[3] A. Inoue, Y. Shinohara, J.S. Gook, Thermal and magnetic properties of bulk Fe-based glassy alloys prepared by copper mold casting, Mater. Trans. JIM 36 (1995) 1427–1433.
[4] A. Inoue, T. Zhang, A. Takeuchi, Bulk amorphous alloys with high mechanical strength and good soft magnetic properties in Fe-TM-B (TM = IV-VIII group transition metal) system, Appl. Phys. Lett. 71 (1997) 464–466.
[5] S.J. Pang, T. Zhang, K. Asami, A. Inoue, Synthesis of Fe-Cr-Mo-C-B-P bulk metallic glasses with high corrosion resistance, Acta Mater. 50 (2002) 489–497.
[6] V. Ponnambalam, S.J. Poon, G.J. Shiflet, Fe-based bulk metallic glasses with diameter thickness larger than one centimeter, J. Mater. Res. 19 (2004) 1320–1323.
[7] P. Duwez, S.C.H. Lin, Amorphous ferromagnetic phase in iron-carbon-phosphorus alloys, J. Appl. Phys. 38 (1967) 4096–4099.
[8] X.J. Gu, S.J. Poon, G.J. Shiflet, Mechanical properties of iron-based bulk metallic glasses, J. Mater. Res. 22 (2007) 345–351.
[9] C. Zhang, L. Liu, K.C. Chan, Q. Chen, C.Y. Tang, Wear behavior of HVOF-sprayed Fe-based amorphous coatings, Intermetallics 29 (2012) 80–85.
[10] J. Schroers, The superplastic forming of bulk metallic glasses, JOM 57 (2005) 35–39.
[11] W. Zhang, H. Guo, M.W. Chen, Y. Saotome, C.L. Qin, New Au-based bulk glassy alloys with ultralow glass transition temperature, Scr. Mater. 61 (2009) 744–747.
[12] W. Zhang, C.F. Fang, Y. Li, Ferromagnetic Fe-based bulk metallic glasses with high thermoplastic formability, Scr. Mater. 69 (2013) 77–80.
[13] A. Inoue, T. Shimizu, S. Yamaura, Y. Fujita, S. Takagi, H. Kimura, Development of glassy alloy separators for a proton exchange membrane fuel cell (PEMFC), Mater. Trans. 46 (2005) 1706–1710.
[14] S. Kim, S. Yamaura, Y. Shimizu, K. Nakashima, T. Igarashi, A. Makino, I. Akihisa, Production of Ni65Cr15P16B4 metallic glass-coated bipolar plate for fuel cell by high velocity oxy-fuel (HVOF) spray coating method, Mater. Trans. 51 (2010) 1609–1613.
[15] T. Xu, S.J. Pang, T. Zhang, Glass formation, corrosion behavior, and mechanical properties of novel Cr-rich Cr-Fe-Mo-C-B-Y bulk metallic glasses, J. Alloys Compd. 625 (2015) 318–322.
[16] Z.L. Long, Y. Shao, X.H. Deng, Z.C. Zhang, Y. Jiang, P. Zhang, B.L. Shen, A. Inoue, Cr effects on magnetic and corrosion properties of Fe-Co-Si-B-Nb-Cr bulk glassy alloys with high glass-forming ability, Intermetallics 15 (2007) 1453–1458.
[17] M.J. Shi, S.J. Pang, T. Zhang, Towards improved integrated properties in FeCrPCB bulk metallic glasses by Cr addition, Intermetallics 61 (2015) 16–20.
[18] X. Li, C.L. Qin, H. Kato, A. Makino, A. Inoue, Mo microalloying effect on the glass-forming ability, magnetic, mechanical and corrosion properties of (Fe0.76Si0.096B0.084P0.06)100-xMox bulk glassy alloys, J. Alloys Compd. 509 (2011) 7688–7691.
[19] S.F. Guo, N. Li, C. Zhang, L. Liu, Enhancement of plasticity of Fe-based bulk metallic glass by Ni substitution for Fe, J. Alloys Compd. 504 (2010) 78–81.
[20] D. Turnbull, Under what conditions can a glass be formed, Contemp. Phys. 5 (1969) 473–488.
[21] Z.P. Lu, C.T. Liu, A new glass-forming ability criterion for bulk metallic glasses, Acta Mater. 50 (2002) 3501–3512.
[22] E. McCafferty, Validation of corrosion rates measured by the Tafel extrapolation method, Corros. Sci. 47 (2005) 3202–3215.
[23] T. Xu, S.J. Pang, H. Li, T. Zhang, Corrosion resistant Cr-based bulk metallic glasses with high strength and hardness, J. Non-Cryst. Solids 410 (2015) 20–25.
[24] T. Xu, Z.Y. Jian, F.G. Chang, L.C. Zhou, M.J. Shi, M. Zhu, J.F. Xu, Y.Q. Liu, T. Zhang, Synthesis of Fe75Cr5(PBC)20 bulk metallic glasses with a combination of desired merits using industrial ferro-alloys without high-purity materials, J. Alloys Compd. 699 (2017) 92–97.
[25] S.H. Sheng, C.L. Ma, S.J. Pang, T. Zhang, Glass-forming ability and mechanical properties of Sm-doped Fe-Cr-Mo-C-B glassy alloys, Mater. Trans. 46 (2005) 2949–2953.
[26] A. Takeuchi, A. Inoue, Calculations of mixing enthalpy and mismatch entropy for ternary amorphous alloys, Mater. Trans. 41 (2000) 1372–1378.
[27] A. Takeuchi, A. Inoue, Classification of bulk metallic glasses by atomic size difference, heat of mixing and period of constituent elements and its application to characterization of the main alloying element, Mater. Trans. 46 (2005) 2817–2829.
[28] J.W. Christian, The Theory of Transformations in Metals and Alloys, Equilibrium and General Kinetic Theory, Pergamon Press, New York, 1975, pp. 15–19.
[29] S.J. Pang, T. Zhang, K. Asami, A. Inoue, Formation of bulk glassy Fe75-x-yCrxMoyC15B10 alloys and their corrosion behavior, J. Mater. Res. 17 (2002) 701–704.
[30] J. Jayaraj, Y.C. Kim, K.B. Kim, H.K. Seok, E. Fleury, Corrosion behaviors of Fe45-xCr18Mo14C15B6Y2Mx (M = Al, Co, Ni, N and x = 0, 2) bulk metallic glasses under conditions simulating fuel cell environment, J. Alloys Compd. 434 (2007) 237–239.
[31] H.J. Ma, W.M. Wang, J. Zhang, G.H. Li, C.D. Cao, H.D. Zhang, Crystallization and corrosion resistance of (Fe0.78Si0.09B0.13)100-xNix (x = 0, 2 and 5) glassy alloys, J. Mater. Sci. Technol. 27 (2011) 1169–1177.
[32] S.F. Guo, N. Li, C. Zhang, L. Lin, Enhancement of plasticity of Fe-based bulk metallic glass by Ni substitution for Fe, J. Alloys Compd. 504 (S1) (2010) S78–S81.
[33] L. Zhang, L.L. Shi, J. Xu, Hf–Cu–Ni–Al bulk metallic glasses: optimization of glass-forming ability and plasticity, J. Non-Cryst. Solids 355 (2009) 1005–1007.